9/1-13-93 JS (2)

PREPARED FOR THE U.S. DEPARTMENT OF ENERGY,
UNDER CONTRACT DE-AC02-76-CHO-3073

PPPL-2873
UC-421

PPPL-2873

Kβ SPECTRA OF HELIUMLIKE IRON FROM TFTR PLASMAS

BY

A.J. SMITH, M. BITTER, K.W. HILL, ET AL.

DECEMBER, 1992

PPPL PRINCETON PLASMA PHYSICS LABORATORY

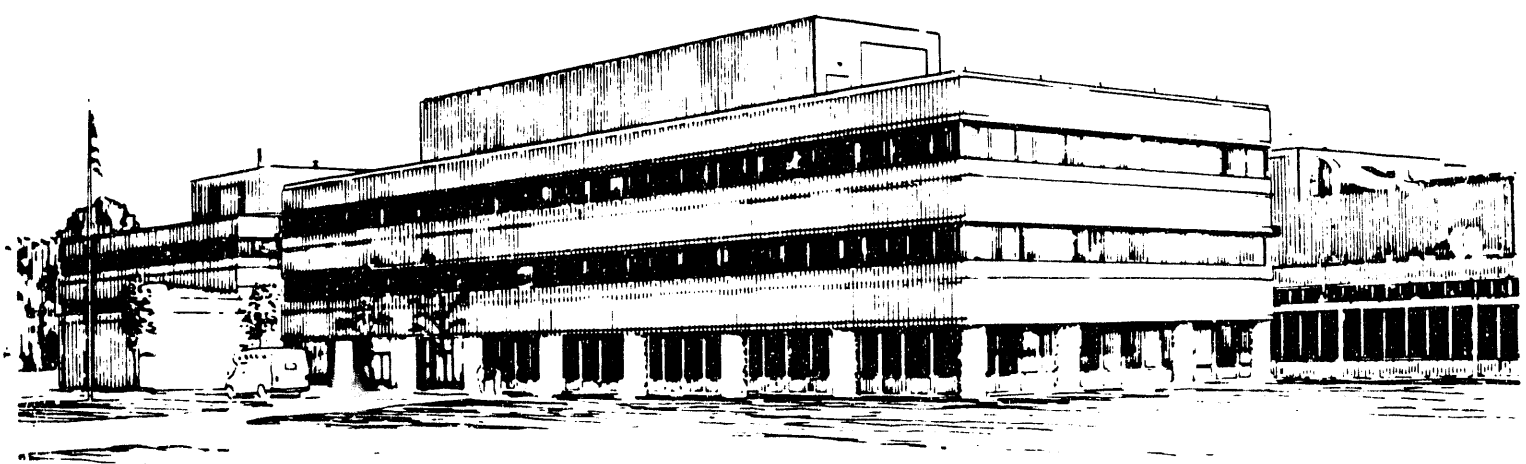

PRINCETON UNIVERSITY, PRINCETON, NEW JERSEY

DISTRIBUTION OF THIS DOCUMENT IS UNLIMITED

NOTICE

This report was prepared as an account of work sponsored by an agency of the United States Government. Neither the United States Government nor any agency thereof, nor any of their employees, makes any warranty, express or implied, or assumes any legal liability or responsibility for the accuracy, completeness, or usefulness of any information, apparatus, product, or process disclosed, or represents that its use would not infringe privately owned rights. Reference herein to any specific commercial produce, process, or service by trade name, trademark, manufacturer, or otherwise, does not necessarily constitute or imply its endorsement, recommendation, or favoring by the United States Government or any agency thereof. The views and opinions of authors expressed herein do not necessarily state or reflect those of the United States Government or any agency thereof.

NOTICE

This report has been reproduced from the best available copy.
Available in paper copy and microfiche.

Number of pages in this report: 25

DOE and DOE contractors can obtain copies of this report from:

Office of Scientific and Technical Information
P.O. Box 62
Oak Ridge, TN 37831;
(615) 576-8401.

This report is publicly available from the:

National Technical Information Service
Department of Commerce
5285 Port Royal Road
Springfield, Virginia 22161
(703) 487-4650

PPPL--2873

DE93 005730

Kß Spectra of Heliumlike Iron from TFTR Plasmas

A. J. Smith

Lock Haven University, Lock Haven, Pa 17745

M. Bitter, H. Hsuan, K. W. Hill, S. von Goeler, and J. Timberlake

Plasma Physics Laboratory, Princeton University, P.O. Box 451, Princeton New Jersey 08543

P. Beiersdorfer and A. Osterheld

Lawrence Livermore National Laboratory, Livermore, CA 94550

MASTER

DISTRIBUTION OF THIS DOCUMENT IS UNLIMITED

Abstract

Kβ spectra of heliumlike iron, Fe XXV, have been observed from TFTR plasmas with a high-resolution crystal spectrometer. The wavelength range of the Fe Kβ spectrum partially overlaps the spectrum of heliumlike nickel (Ni XXVII), which is used on TFTR and JET for ion temperature measurements. The experimental arrangement made it possible to observe the Fe XXV Kβ lines and their satellite transitions of the type 1s2l'3l'' --> $1s^2 2l'$, as well as the entire satellite spectrum of the Ni XXVII Kα line simultaneously. In order to identify the features of the Kβ spectra and to study their possible interference with the Ni XXVII spectrum, the intensity of the Kβ spectrum was enhanced by injection of iron into the plasma. Accurate wavelengths and intensities have been obtained and compared with different theoretical calculations.

*Supported by DOE Contract No. DE-AC02-76-CHO-3073

I. Introduction

High resolution satellite spectra of high-Z atoms are important for the diagnostics of tokamak plasmas and solar flares, and they are also of interest in testing atomic theories which must include relativistic and quantum electrodynamics effects. In the large tokamaks such as the Tokamak Fusion Test Reactor (TFTR), the Joint European Torus (JET), the large Japanese tokamak JT-60 U, and Tore Supra, where large volume (>40m^3) plasmas with peak electron temperatures ~ 5 keV are maintained for several seconds, hydrogenlike and heliumlike ions of high-Z atoms such as titanium, chromium, iron, and nickel, are readily produced. Line radiation from these highly stripped ions is used for electron and ion temperature diagnostics as well as for determination of charge-state distributions and ion transport coefficients. In particular, the resonance line of heliumlike nickel[1-4] is employed on TFTR, JET and Tore Supra for Doppler broadening and Doppler shift measurements in order to determine the central ion temperature as well as toroidal and poloidal plasma velocities.

In the case of TFTR and Tore Supra which use stainless steel (~ 70 at. % Fe, ~ 20 at. % Cr, ~ 7 at. % Ni) walls and Inconel (~ 70 at. % Ni, ~15 at. % Cr, ~7 at. % Fe, ~2.5 at. % Ti) bellows protective cover plates, iron and nickel are simultaneously present as wall-derived impurities. Thus the possibility exists that the FeXXV Kβ spectrum and the NiXXVII Kα spectrum, which fall in the wavelength range from 1.57 to 1.62 Å, interfere with each other. It is therefore of considerable interest to determine whether a distortion of the Ni Kα spectrum by the Fe Kβ spectrum impairs the ion temperature measurements. In this paper, we investigate the Kβ spectrum of heliumlike iron. Such a study is very important since experimental data on Kβ spectra are scarce.

Under normal TFTR operating conditions prior to 1987, when the present data were collected, the nickel Kα radiation was much more intense than the iron Kβ radiation.[5] Iron was therefore injected into the plasma by a laser blow-off technique in order to enhance the iron Kβ emission relative to the nickel Kα emission. Thus it was possible to extract the Fe Kβ spectrum from the obtained composite spectrum and to clearly identify most of the theoretically predicted features.

The experimental wavelengths of the Kβ lines and the associated satellite features were determined relative to the positions of nickel Kα lines with an accuracy of ~ 0.1 mÅ.

An important result of our experiments is that the $K\beta$ features are found to be well separated from the nickel $K\alpha$ resonance line, so that there is no interference with the central ion temperature measurement. As an additional benefit, observation of the time history of the $K\beta$ radiation following the iron injection makes it possible to study the confinement of metal impurity ions in TFTR plasmas.

The paper is organized as follows: Section II presents theoretical data on the iron $K\beta$ satellite spectrum obtained from the Hebrew University-Lawrence Livermore Atomic Code (HULLAC) package. The experimental results and data analysis are described in Section III. Conclusions are given in Section IV.

II. Theory

The spectrum of interest includes the $K\beta$ lines of heliumlike iron, corresponding to the transitions $1s^2\ {}^1S_0$ - $1s3p\,{}^1P_1$ and $1s^2\ {}^1S_0$ - $1s3p\ {}^3P_1$, and the associated lithiumlike and berylliumlike satellites due to the transitions: $1s^22l$ - $1s2l'3l''$ and $1s^22s2l'$ - $1s2s2l'3l''$. These satellites can be formed (1) in the process of dielectronic recombination of heliumlike or lithiumlike ions or (2) by collisional inner-shell excitation of lithiumlike and berylliumlike ions from their ground states. In the first process a free electron is captured by a heliumlike <u>or</u> lithiumlike ion into the $n = 3$ level :

$$1s^2 + e^- \rightarrow 1s2l'3l'', \tag{1}$$

<u>or</u>

$$1s^22s + e^- \rightarrow 1s2s2l'3l''. \tag{2}$$

The resulting autoionizing states given in Eq. (1) can decay by two types of radiative decay schemes :

$$1s2l'3l'' \rightarrow 1s^23l, \tag{3}$$

or

$$1s2l'3l'' \rightarrow 1s^22l\,. \tag{4}$$

The first type provides satellites to the heliumlike Kα resonance line. These, so-called unresolved n=3 satellites, lie very close to the Kα resonance line and have been investigated rather well.[6] Of interest for the present paper are the transitions of the second type which give rise to n = 2 satellites of the Kβ lines. Because the plasma also contains lithiumlike ions, we expect to find satellite transitions from the dielectronic recombination of lithiumlike ions by radiative decay of the excited states given in Eq. (2):

$$1s^2 2s + e^- \rightarrow 1s2s2l'3l'' \rightarrow 1s^2 2s2l'. \tag{5}$$

The relevant transitions due to the second process of direct electron-impact excitation of inner-shell electrons from lithiumlike and berylliumlike charge states involve only the ground states of these ions:

$$1s^2 2s + e^- \rightarrow 1s2s3l + e^- \tag{6}$$

and

$$1s^2 2s^2 + e^- \rightarrow 1s2s^2 3l + e^-, \tag{7}$$

since the so-called zero-density limit applies to the low electron densities of TFTR plasmas.

In the following, we discuss the line emissivities for ions from different charge states. The emissivities of the heliumlike Kβ lines can be represented by

$$\varepsilon_{He} = N_e N_{He} C \tag{8}$$

where N_e and N_{He} are the electron and heliumlike ion densities and C is an effective excitation rate coefficient which takes into account direct excitation and radiative cascades. These rate coefficients were obtained with the HULLAC set of atomic codes, which calculate wave functions, energy levels, and radiative transition rates by the relativistic, multi-configuration parametric potential method with full configuration interaction.[7] The collisional excitation rates were calculated in the distorted-wave approximation; an efficient technique, which performs an angular factorization of both the direct and exchange contributions to excitation cross sections and interpolates the necessary radial integrals as a function of threshold energy[8] was used. The excitation

rate coefficients obtained from these calculations are given in Table I as a function of the electron temperature.

The emissivities of the so-called collisional satellites lines which result from inner-shell electron impact excitation of the lithiumlike and berylliumlike charge states are given by

$$\varepsilon_{cs} = N_e N_{Li(Be)} C \frac{A_r^{sf}}{\sum_f A_r^{sf} + \sum_i A_a^{si}} \tag{9}$$

where $N_{Li(Be)}$ is the density of the lithiumlike or berylliumlike charge state, A_r^{sf} is the radiative transition probability for the transition in question, and A_a^{si} is the autoionization probability to some final state i. The excitation rate coefficients C for the lithiumlike and berylliumlike ions were obtained by the same methods as were the rate coefficients for the heliumlike ions , while the autoionization rates were obtained from a factorization-interpolation technique using a single consistent potential for the bound and continuum orbitals.[9] The excitation rate coefficients and transition probabilities for Fe XXIV and Fe XXIII are also listed in Table I.

The emissivities of the lithiumlike dielectronic satellites of the Kβ lines can be represented by

$$\varepsilon_d = N_e N_{He} F_1^*(T_e) F_2^*(s) \ , \tag{10}$$

where the factor

$$F_1^*(T_e) = \tfrac{1}{2}\left[\frac{2\pi\hbar}{mkT_e}\right]^{1/2} \exp(-E_s/kT_e) \tag{11}$$

depends only on the electron temperature, and

$$F_2(s) = \frac{g_s}{g_i} \frac{A_r^{sf} A_a^{si}}{\sum_i A_a^{si} + \sum_f A_r^{sf}} \tag{12}$$

is the line strength. Here g_s and g_i are the statistical weights of the autoionizing states and the ground states, respectively, and E_s is the energy of the satellite level above that of the heliumlike ground state. The emissivities of the berylliumlike dielectronic satellite lines are given by an expression similar to (4) except that N_{He} is replaced by N_{Li}. The intensity factors $F_2(s)$ for the strong lithiumlike and berylliumlike dielectronic satellites calculated with the HULLAC package are listed in Tables II and III, respectively.

III. Experimental Results.

The spectra were obtained from five nearly identical ohmically heated TFTR discharges with the following parameters: The plasma current and the toroidal magnetic field were I_p = 1.4 MA and B_T = 3.2 T, and the plasma major and minor radii were R = 2.48 m and a = 0.80 m. These discharges were in steady-state conditions during the period from 1.5 to 4.5 s and had a peak electron temperature of 2.7 keV and a peak electron density of 4.3 x 10^{13} cm^{-3}. Figure 1 shows the time evolution of the electron temperature T_e and electron density N_e for the TFTR discharge number 28931, which is typical of the discharges used in this experiment. The electron temperature and density data were obtained from electron cyclotron measurements and laser interferometry. Iron was injected into the plasma at 2.7 s by a laser blow-off technique. The injection led to a substantial increase (30 %) of the total radiated power, but did not affect the central electron temperature and electron density, see Fig. 1.

The spectral data were recorded with the TFTR horizontal and vertical curved crystal spectrometers.[10,11] The horizontal spectrometer was used to measure the composite spectra of the NiXXVII Kα and the FeXXV Kβ radiation. This spectrometer permits observation of spectral features in the wavelength range 1.57 to 1.62 Å, with a spectral resolving power of $\lambda/\Delta\lambda$ = 7500. The vertical spectrometer was used for simultaneous observation of the FeXXV Kα spectrum near 1.85 Å. Both spectrometers recorded 128 spectra from a discharge with a time resolution of 10 ms per spectrum, starting at 2.5 s.

Figure 2 shows the time history of the FeXXV Kα and Kβ line intensities. These line intensities reach a maximum at 2.770 s, i.e. 70 ms after the injection of iron. The intensities then decay exponentially with an e-folding time of 300 ms, which is a measure of the particle confinement time. A more detailed understanding of these data requires

plasma modeling calculations, e. g. with the Multi-Ion Species Transport (MIST) code,[12] which takes into consideration the processes of ionization and recombination as well as ion transport due to diffusion and convection.

Figure 3 presents composite satellite spectra of the iron Kβ and nickel Kα lines from different time periods: (a) the period from 2.5 to 2.7 s before the injection of iron, and (b) the period from 2.75 to 2.88 s after injection, when the radiation from the injected iron is greater than 50% of its maximum value (see Fig. 2). The satellite spectrum of the NiXXVII Kα line has been described earlier by Hsuan et al.[1] and by Bitter et al.[4] The dominant features of the FeXXV Kβ spectrum, the $1s^2\ {}^1S_0$ - $1s3p\,{}^1P_1$ and $1s^2\ {}^1S_0$ - $1s3p\ {}^3P_1$ transitions, are on the short wavelength side of the NiXXVII Kα line between channels 140 and 160. It is evident from Figs. 3 (a) and (b) that the iron Kβ spectrum is very weak compared to the nickel spectrum under normal operating conditions in TFTR, but that it is enhanced by an order of magnitude following the iron injection. The second spectrum, Fig. 3(b), also shows some Kβ satellite lines in the neighborhood of the nickel Kα line **w** and in the wavelength range of the nickel features **x**, **s** and **t**, see Gabriel's notation.[13] These features are not apparent in Fig. 3(a). The nickel resonance line **w**, the dielectronic satellite line **j** and the combined lines **q** and **y**, as well as **l**, β and **z** (see Gabriel's notation[13]) are not distorted by the iron lines, even during strong iron injection.

Since the electron temperature T_e and the electron density N_e were not affected by the iron injection, the nickel spectrum of Fig. 3(a) can be normalized and subtracted from the composite nickel-iron spectrum of Fig. 3(b). The experimental iron Kβ spectrum obtained in this way is shown in Fig. 4(a). The main features of the observed spectrum include the Kβ_1 and Kβ_2 lines (labeled 1 and 2) and the more prominent satellite transitions 3 through 9 which are identified in Table 4. In order to determine wavelengths of the observed spectrum accurately, the central channel numbers for the prominent peaks have been obtained by a least squares fit of Voigt profiles to the experimental data. These central channel numbers have then been converted to wavelengths using the equation

$$\lambda = 2d\sin(\theta_0 + \Delta\theta), \tag{13}$$

where 2d = 2.028 Å is the 2d-spacing of the quartz crystal (cut: 2243) and $\Delta\theta$ (deg) = $9.6880\times10^{-3}(N-N_0)$ is the dispersion of the instrument. N_0 and θ_0 are the channel number and the Bragg angle for the nickel line **w**. Since the spectrometer has no

absolute wavelength calibration, the theoretical wavelength value of 1.5884 Å for the nickel w line from Safronova's calculations[14] is used as a reference value, i. e. we assigned $\lambda_0^{theor} = 1.5884 = 2d\sin(\theta_0)$ to channel number N_0. The experimental wavelengths of the prominent features are shown in Table 4 together with the theoretical wavelengths of the present calculations, see Tables II and III, and those from the calculations by Safronova,[14] Chen[15] and Nilsen.[16] Safronova uses the 1/Z expansion perturbation technique, with relativistic corrections taken into account within the framework of the Breit operator. Chen[15] computes the relevant atomic data relativistically in intermediate coupling using configuration interaction in the multi-configuration Dirac-Fock model (MCDF); a generalized Breit interaction and QED corrections were also taken into account . The third set of calculations by Nilsen uses MCDF for bound states and distorted-wave Dirac continuum states for electrons.

The different sets of theoretical wavelengths listed in Table 4 are in good general agreement with the experimental wavelengths, given that these wavelengths can be shifted by a constant amount due to the fact that the spectrometer is not absolutely calibrated. The wavelengths of Safronova's calculations seem to be more consistent with the observed data; the wavelengths from our calculations tend to be smaller than the observed values by about 0.3 m$\mathring{A}$, while those from Chen and Nilsen tend to be 0.2 and 0.7 m$\mathring{A}$, respectively, larger than the observed data.

Figure 4(b) shows a synthetic FeXXV Kβ spectrum constructed from the present theoretical data. The additional parameters, i. e. the electron and ion temperatures, T_e and T_i, as well as the relative densities, N_{He}, N_{Li} and N_{Be}, of the heliumlike, lithiumlike, and berylliumlike charge states of iron, have been derived from the iron Kα spectrum which was observed with the vertical TFTR spectrometer. The synthetic spectrum shown in Fig. 4(b) was obtained using Te = 2.7 keV, Ti = 3.0 keV, and with N_{He}, N_{Li} and N_{Be} in the ratio of 1.0 : 0.55 : 0.11.

IV Conclusions.

The Fe XXV Kβ spectrum has been obtained from TFTR discharges and found to be in good agreement with a synthetic spectrum constructed from new theoretical predictions. Since the iron Kβ spectrum was partially blended with the Ni XXVII Kα spectrum, it was necessary to enhance the intensity of the Kβ radiation by the injection of iron into

the plasma. A total of nine features in the Fe XXV Kβ spectrum have been identified. The relative intensities depend on the electron temperature and charge state balance, which suggests their future use for plasma diagnostics.

Experimental wavelengths of the FeXXV Kβ spectrum have been determined relative to the Ni XXVII Kα resonance line. The satellite lines of the iron Kβ spectrum do not interfere with the Ni XXVII Kα resonance line. This is important for both TFTR and Tore Supra plasmas where iron and nickel are simultaneously present as impurities and where the Ni XXVII Kα line is used for ion temperature measurements.

Acknowledgments. We deeply appreciate the fruitful discussions with Professor U. I. Safronova and would like to thank her for making her most recent wavelength calculations for the FeXXV Kβ spectrum available to us. We also gratefully acknowledge the continuing support of D. Meade, R. J. Hawryluk and K. M. Young, the technical assistance of J. Gorman, R. Such and the TFTR operating crew, and software support by N. Schechtman. This work was supported by the U.S. Department of Energy, Contract No. DE-AC02-76-CHO-3073 and Contract No. W-7405-Eng-48.

References

(1) H. Hsuan, M. Bitter, K. W. Hill, S. von Goeler, B. Grek,, D. Johnson, L. C. Johnson, S. Sesnic, C. P. Bhalla, K. B. Karim, F. Bely-Dubau and P. Faucher, Phys. Rev. A 35, 4280(1987).

(2) F. Bombarda, R. Giannela, E. Källne, G. J. Tallents, F. Bely-Dubau, P. Faucher, M. Cornille, J. Dubau and A. H. Gabriel, Phys. Rev. A 37, 504(1988); and H. Hsuan, M. Bitter, J. E. Rice, K. W. Hill, L. Johnson, S. L. Liew, S. D. Scott, and S. von Goeler, Rev. Sci. Instrum. 59, 2127(1988).

(3) F. Bombarda, R. Giannella, E. Källne, G. J. Tallents, J. Quant. Spectrosc. Radiat. Transf. 41, 323(1989).

(4) M. Bitter, H. Hsuan, V. Decaux, B. Grek, K. W. Hill, R. Hulse, L. A. Kruegel, D. Johnson, S. von Goeler and M. Zarnstoff, Phys. Rev. A 44, 1796(1991).

(5) In 1987 the Inconel bellows cover plates were covered with graphite tiles, so that the concentration of nickel was very much reduced and iron became the dominant metal impurity in TFTR discharges. Line radiation from nickel could then no longer be used for ion temperature measurements and the spectrometer was realigned for the observation of the FeXXV $K\alpha$ line.

(6) F. Bely-Dubau, A. H. Gabriel and S. Volonte, Mon. Not. R. Astr. Soc. 186,405(1979); and M. Bitter, S. von Goeler, K. W. Hill, R. Horton, D. Johnson, W. Roney, N. Sauthoff, E. Silver and W. Stodiek, Phys. Rev. Lett. 47, 921(1981).

(7) M. Klapisch, Comput. Phys. Commun. 2, 239(1971); and M. Klapisch, J. L. Schwob, B. S. Fraenkel, and J. Oreg, J. Opt. Soc. Am. 61, 148(1977).

(8) A. Bar-Shalom, M. Klapisch, and J. Oreg, Phys. Rev. A 38 , 1773(1988).

(9) J. Oreg, A. Bar-Shalom, W. H. Goldstein, and M. Klapisch, Phys. Rev. A 44,1750(1991).

(10) M. Bitter, K. W. Hill, S. Cohen, S. von Goeler, H. Hsuan, L. C. Johnson, R. Raftopoulos, M. Reale, N. Schechtman, F. Spinos, J. Timberlake, N. Young and K. M. Young, Rev. Sci. Instrum. 57, 2145(1986).

(11) K. W. Hill, M. Bitter, M. Tavernier, M. Diesso, S. von Goeler, G. Johnson, L. C. Johnson, N.. Sauthoff, N. Schechtman, S. Sesnic, F. Tenney and K. M. Young, Rev. Sci. Instrum. 56, 1165(1985).

(12) R. A. Hulse, Nucl. Technol. Fusion 3, 259 (1983).

(13) A. H. Gabriel, Mon. Not. R. Astr. Soc. 160, 79(1972).

(14) U. I. Safronova, personal communication, 1992.

(15) M. H. Chen, Atomic Data and Nuclear Data Tables 34, 301(1986).

(16) J. Nilsen, Atomic Data and Nuclear Data Tables 37,191(1987)

Table I: Excitation rate coefficients,for direct electron impact excitation from the ground states of (a) FeXXV, FeXXI, and (b) FeXXIII at electron temperatures between 1.2 and 4.0 keV. Also listed are the autoinization probabilities A_a^{si}, the radiative transition probabilities A_r, and the branching ratios defined as $\beta_r = \frac{A_r^{sf}}{\sum_f A_r^{sf} + \sum_i A_a^{si}}$. The numbers in square brackets are powers of ten.

Table II: Intensity factors for the lithiumlike dielectronic satellite lines of the iron $K\beta$ lines; only lines with line factors larger than 1% of the strongest satellite are listed. Numbers in square brackets signify powers of 10.

Table III: Intensity factors for the berylliumlike satellites of the iron $K\beta$ lines; only lines with $F_2(s) \geq 2.0x10^{12} s^{-1}$ are included. Numbers in square brackets signify powers of 10.

Table IV: Experimental wavelengths and theoretical predictions for the lines in the iron $K\beta$ spectrum; peaks are numbered as in Fig 6.

Table Ia

Charge State	Excited State	λ_{Theor} [a]	A_a (s^{-1})	A_r (s^{-1})	β_r	Excitation Rate Coefficients for FeXXV and EeXXIV at different Electron Temperatures				
						1.5 keV	2.0 keV	2.5 keV	3.0 keV	3.5 keV
FeXXV	$[1s3p_{3/2}]_1$	1.5732	0	1.3985[14]	0.940	5.974[-15]	2.077[-14]	4.370[-14]	7.161[-14]	1.018[-13]
	$[1s3p_{1/2}]_1$	1.5751	0	1.0757[13]	0.546	1.807[-15]	5.635[-15]	1.080[-14]	1.633[-14]	2.163[-14]
FeXXIV	$[1s2s3p_{3/2}]_{3/2}$	1.5853	5.8017[12]	4.8657[13]	0.608	1.842[-15]	6.159[-15]	1.258[-14]	2.015[-14]	2.813[-14]
	$[1s2s3p_{1/2}]_{1/2}$	1.5864	5.0193[11]	6.1784[13]	0.813	1.060[-15]	3.596[-15]	7.436[-15]	1.293[-14]	1.693[-14]
	$[1s2p_{1/2}3s]_{3/2}$	1.5878	1.0177[12]	1.0134[13]	0.252	3.078[-16]	1.054[-15]	2.194[-15]	3.571[-15]	5.051[-15]
	$[1s2p_{1/2}3s]_{1/2}$	1.5886	2.9939[11]	4.1506[12]	0.309	6.324[-17]	2.128[-16]	4.373[-16]	7.039[-16]	9.866[-16]
	$[1s2s3p_{3/2}]_{1/2}$	1.5912	1.3235[12]	6.9929[13]	0.813	1.178[-15]	3.979[-15]	8.202[-15]	1.324[-14]	1.860[-14]
	$[1s2s3p_{3/2}]_{3/2}$	1.5913	1.7645[12]	6.3381[13]	0.738	2.302[-15]	7.728[-15]	1.586[-14]	2.549[-14]	3.572[-14]
	$[1s2s3p_{1/2}]_{3/2}$	1.5924	6.5669[12]	1.6307[13]	0.786	1.376[-15]	4.310[-15]	8.337[-15]	1.274[-14]	1.706[-14]
	$[1s2s3p_{1/2}]_{1/2}$	1.5926	1.2161[11]	3.4637[13]	0.776	5.423[-16]	1.631[-15]	3.035[-15]	4.469[-15]	5.779[-15]

Table Ib

Charge State	Excited State	λ_{Theor} [a] (Å)	A_a (s^{-1})	A_r (s^{-1})	β_r	Excitation Rate Coefficients for FeXXIII at differentElectron Temperatures				
						1.2 keV	1.6 keV	2.0 keV	3.0 keV	4.0 keV
FeXXIII	$[1s2s^2 3p_{3/2}]_1$	1.6053	6.9341[11]	1.2430[14]	0.852	1.67441[-15]	7.801[-15]	1.956[-14]	6.635[-14]	1.220[-13]

Table II

Transition	λ_{Theor} (Å)	gs	Aa (s^{-1})	β r	F2(s) (s^{-1})
$[1s2s3p_{3/2}]_{3/2} - 1s^2 2s$	1.5853	4	5.80[12]	0.608	1.41[13]
$[1s2p_{3/2}3p_{3/2}]_{3/2} - 1s^2 2p_{3/2}$	1.5900	4	1.66[13]	0.100	6.64[12]
$[1s2p_{3/2}3p_{3/2}]_{5/2} - 1s^2 2p_{3/2}$	1.5907	6	3.30[13]	0.048	9.50[12]
$[1s2p_{3/2}3p_{1/2}]_{3/2} - 1s^2 2p_{3/2}$	1.5912	4	3.96[13]	0.050	7.92[12]
$[1s2s3p_{3/2}]_{1/2} - 1s^2 2s$	1.5912	2	1.32[12]	0.813	2.15[12]
$[1s2s3p_{3/2}]_{3/2} - 1s^2 2s$	1.5913	4	1.76[12]	0.738	5.20[12]
$[1s2p_{3/2}3p_{1/2}]_{3/2} - 1s^2 2p_{1/2}$	1.5922	4	3.38[12]	0.157	2.12[12]
$[1s2s3p_{1/2}]_{3/2} - 1s^2 2s$	1.5924	4	6.70[11]	0.786	2.10[12]
$[1s2p_{1/2}3p_{3/2}]_{3/2} - 1s^2 2p_{3/2}$	1.5931	6	3.12[13]	0.663	1.24[14]
$[1s2p_{1/2}3p_{3/2}]_{3/2} - 1s^2 2p_{1/2}$	1.5933	4	9.02[12]	0.523	1.88[13]
$[1s2p_{3/2}3p_{3/2}]_{3/2} - 1s^2 2p_{3/2}$	1.5946	4	4.78[12]	0.419	8.01[12]
$[1s2p_{3/2}3p_{1/2}]_{5/2} - 1s^2 2p_{3/2}$	1.5949	6	6.49[12]	0.305	1.19[13]
$[1s2p_{3/2}3p_{1/2}]_{3/2} - 1s^2 2p_{3/2}$	1.5954	4	3.38[12]	0.362	4.89[12]
$[1s2s3d_{5/2}]_{3/2} - 1s^2 2p_{1/2}$	1.5980	4	4.50[12]	0.230	4.14[12]
$[1s2s3d_{5/2}]_{5/2} - 1s^2 2p_{3/2}$	1.6013	6	3.76[12]	0.122	2.75[12]
$[1s2s3s_{1/2}]_{1/2} - 1s^2 2p_{1/2}$	1.6034	2	4.33[13]	0.052	4.50[12]
$[1s2s3s_{1/2}]_{1/2} - 1s^2 2p_{3/2}$	1.6067	2	4.33[13]	0.054	4.68[12]

Table III

Transitions	λ_{Theeor} (Å)	g_s	$A_a^{s\to 0}$ (s^{-1})	β_r	$F_2(s)$ (s^{-1})
$[1s2s2p_{3/2}3p_{3/2}]_3-[1s^22s2p_{3/2}]_2$	1.6023	7	1.16[13]	0.112	4.55[12]
$[1s2s2p_{3/2}3p_{3/2}]_2-[1s^22s2p_{3/2}]_2$	1.6027	5	2.11[13]	0.054	2.85[12]
$[1s2s2p_{1/2}3p_{3/2}]_2-[1s^22s2p_{1/2}]_1$	1.6047	5	1.09[13]	0.107	2.92[12]
$[1s2s2p_{3/2}3p_{3/2}]_3-[1s^22s2p_{3/2}]_2$	1.6052	7	1.84[13]	0.081	5.22[12]
$[1s2s2p_{3/2}3p_{3/2}]_0-[1s^22s2p_{3/2}]_1$	1.6057	1	1.43[13]	0.367	2.62[12]
$[1s2s2p_{3/2}3p_{3/2}]_2-[1s^22s2p_{3/2}]_1$	1.6071	5	1.56[13]	0.281	1.10[13]
$[1s2s2p_{3/2}3p_{1/2}]_2-[1s^22s2p_{3/2}]_1$	1.6082	5	2.99[13]	0.326	2.44[13]
$[1s2s2p_{3/2}3p_{3/2}]_2-[1s^22s2p_{1/2}]_1$	1.6095	5	1.81[13]	0.153	6.92[12]
$[1s2s2p_{3/2}3p_{3/2}]_1-[1s^22s2p_{3/2}]_2$	1.6101	3	8.76[12]	0.503	6.61[12]
$[1s2s2p_{1/2}3p_{3/2}]_1-[1s^22s2p_{1/2}]_0$	1.6102	3	2.53[13]	0.148	5.62[12]
$[1s2s2p_{3/2}3p_{1/2}]_2-[1s^22s2p_{1/2}]_1$	1.6106	5	3.38[12]	0.271	2.29[12]
$[1s2s2p_{1/2}3p_{3/2}]_3-[1s^22s2p_{3/2}]_2$	1.6108	7	3.08[13]	0.614	6.62[13]
$[1s2s2p_{1/2}3p_{3/2}]_1-[1s^22s2p_{1/2}]_1$	1.6110	3	2.53[13]	0.425	1.61[13]
$[1s2s2p_{1/2}3p_{3/2}]_2-[1s^22s2p_{1/2}]_1$	1.6115	5	5.72[12]	0.361	5.16[12]
$[1s2s^23d_{5/2}]_3-[1s^22s2p_{1/2}]_1$	1.6116	5	4.22[12]	0.445	4.69[12]
$[1s2s2p_{3/2}3p_{3/2}]_2-[1s^22s2p_{3/2}]_2$	1.6119	5	1.81[13]	0.459	2.08[13]
$[1s2s2p_{1/2}3p_{3/2}]_1-[1s^22s2p_{1/2}]_0$	1.6120	3	4.04[12]	0.602	3.65[12]
$[1s2s2p_{3/2}3p_{1/2}]_3-[1s^22s2p_{3/2}]_2$	1.6125	7	5.83[12]	0.442	9.02[12]
$[1s2s2p_{3/2}3p_{1/2}]_2-[1s^22s2p_{3/2}]_2$	1.6130	5	3.38[12]	0.311	2.63[12]
$[1s2s2p_{3/2}3p_{1/2}]_2-[1s^22s2p_{3/2}]_1$	1.6130	5	2.73[13]	0.039	2.66[12]

Table IV

Peak	Transitions	Channel Number	λ_{Exprt} (Å)	λ_{Theor} (Å)	λ_a (Å)	λ_b (Å)	λ_c (Å)
1	$1s3p\,^1P_1$-$1s^2\,^1S_0$	138.07	1.5734	1.5732	1.5732	1.57396	
2	$1s3p\,^3P_1$-$1s^2\,^1S_0$	146.02	1.5751	1.5751	1.5751	1.57584	
3	$1s2s[^1S]3p\,^2P_{3/2}$-$1s^22s\,^2S_{1/2}$	194.32	1.5854	1.5853	1.5855	1.58593	1.5858
4	$1s2s[^1S]3p\,^2P_{1/2}$-$1s^22s\,^2S_{1/2}$	200.0	1.5867	1.5864	1.5866		1.5869
w*	$1s2p\,^1P_1 - 1s^2\,^1S_0$	**208.14**	**1.5884**		**1.5884**		
5	$1s2s[^3S]3p\,^2P_{1/2}$-$1s^22s\,^2S_{3/2}$	222.16	1.5914	1.5912	1.5915	1.59190	1.5917
	$1s2s[^3S]3p\,^2P_{1/2}$-$1s^22s\,^2S_{1/2}$			1.5913	1.5916	1.5919	1.5918
6	$1s2p[^3P]3p\,^2D_{5/2}$-$1s^22p\,^2P_{3/2}$	230.68	1.5932	1.5931	1.5934	1.59387	1.5935
7	$1s2p[^3P]3p\,^2P_{5/2}$-$1s^22p\,^2P_{3/2}$	239.11	1.5950	1.5949	1.5951	1.59567	1.5954
z*	$1s2s\,^3S_1 - 1s^2\,^1S_0$	**279.80**	**1.6036**		**1.6037**		
8	$1s2s^23p\,^1P_1$-$1s^22s\,^1S_0$	289.42	1.6056	1.6053	1.6055		
9	$1s2s2p3p\,^3P_1$-$1s^22s2p\,^3P_2$	315.02	1.6109	1.6108			

*w and z lines of NiXXVII

λ_{Theor} from present calculations

λ_a from Ref. 14

λ_b from Ref. 16

λ_c from Ref. 15

Figure Captions

Figure 1: Electron temperature and electron density as functions of time for TFTR shot 28931. The data were obtained from measurements of the electron cyclotron emission and laser interferometry. Iron was injected at 2.7 s by a laser ablation technique.

Figure 2: Time history of (a) the Fe Kβ and (b) the Fe Kα line intensities.

Figure 3: Satellite spectra of Ni XXVII Kα and Fe XXV Kβ (a) before and (b) after iron injection. The data have been accumulated from five nearly identical TFTR ohmic shots during the periods 2.5 - 2.7 s for Fig. 3 (a) and 2.75 - 2.88 s for Fig. 3 (b). The features of the Ni XXVII Kα satellite spectrum have been identified using Gabriel's notation.[13] The Fe XXV Kβ features are significantly enhanced in the spectrum (b) which was recorded after iron injection.

Figure 4: (a) Experimental iron Kβ spectrum obtained by subtracting a normalized spectrum of Fig. 3 (a) from the spectrum shown in Fig. 3 (b). (b) Synthetic iron Kβ spectra constructed from present theoretical data for the measured electron and ion temperatures of T_e = 2.7 keV and T_i = 2.35 keV. The shaded area represents the satellite contributions from collisional inner-shell excitation. The solid line represents the entire spectrum including contributions from dielectronic recombination.

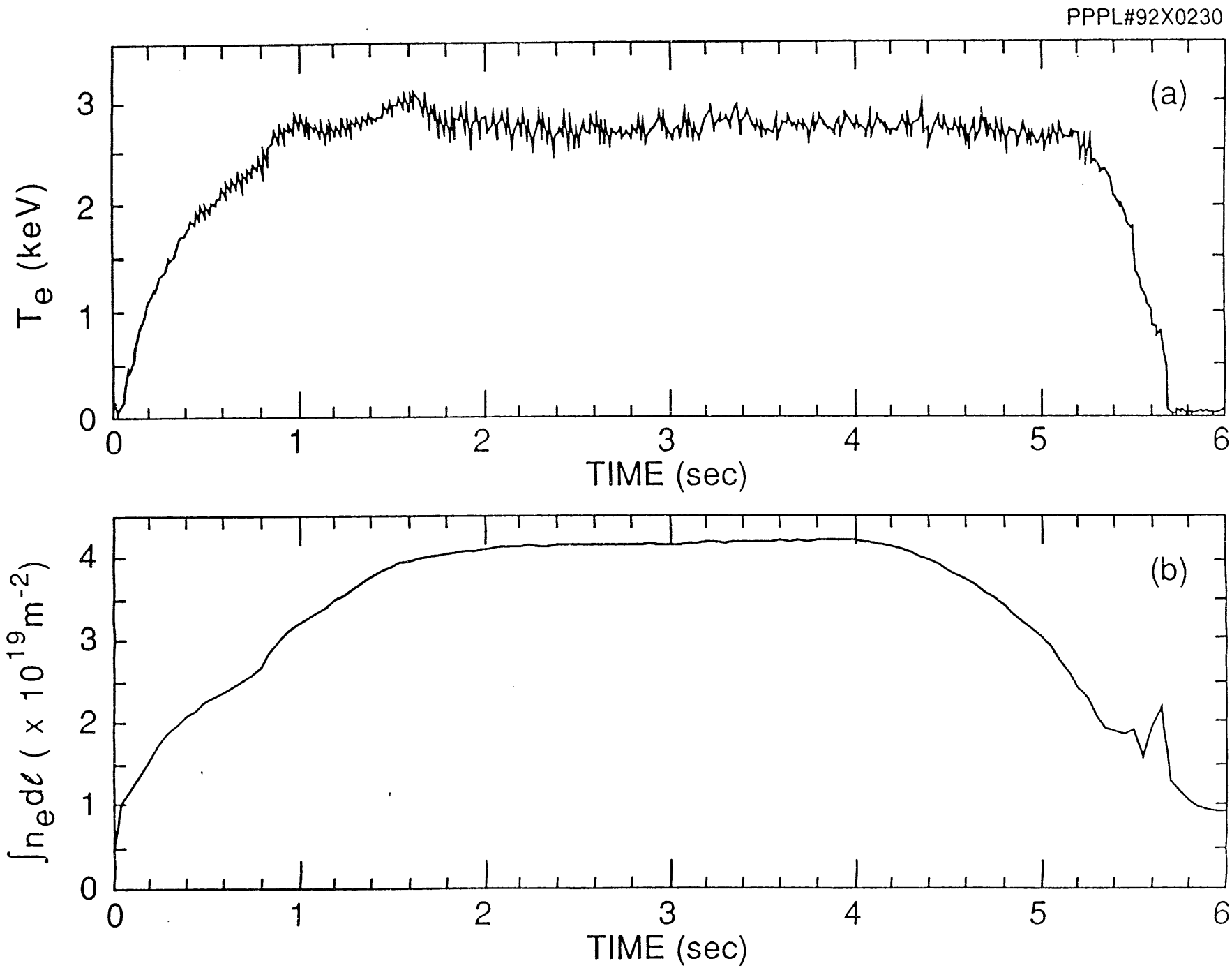
PPPL#92X0230
(a)
T_e (keV)
0
1
2
3
0
1
2
3
4
5
6
TIME (sec)
(b)
$\int n_e d\ell$ (x 10^{19} m^{-2})
0
1
2
3
4
0
1
2
3
4
5
6
TIME (sec)

Figure 1

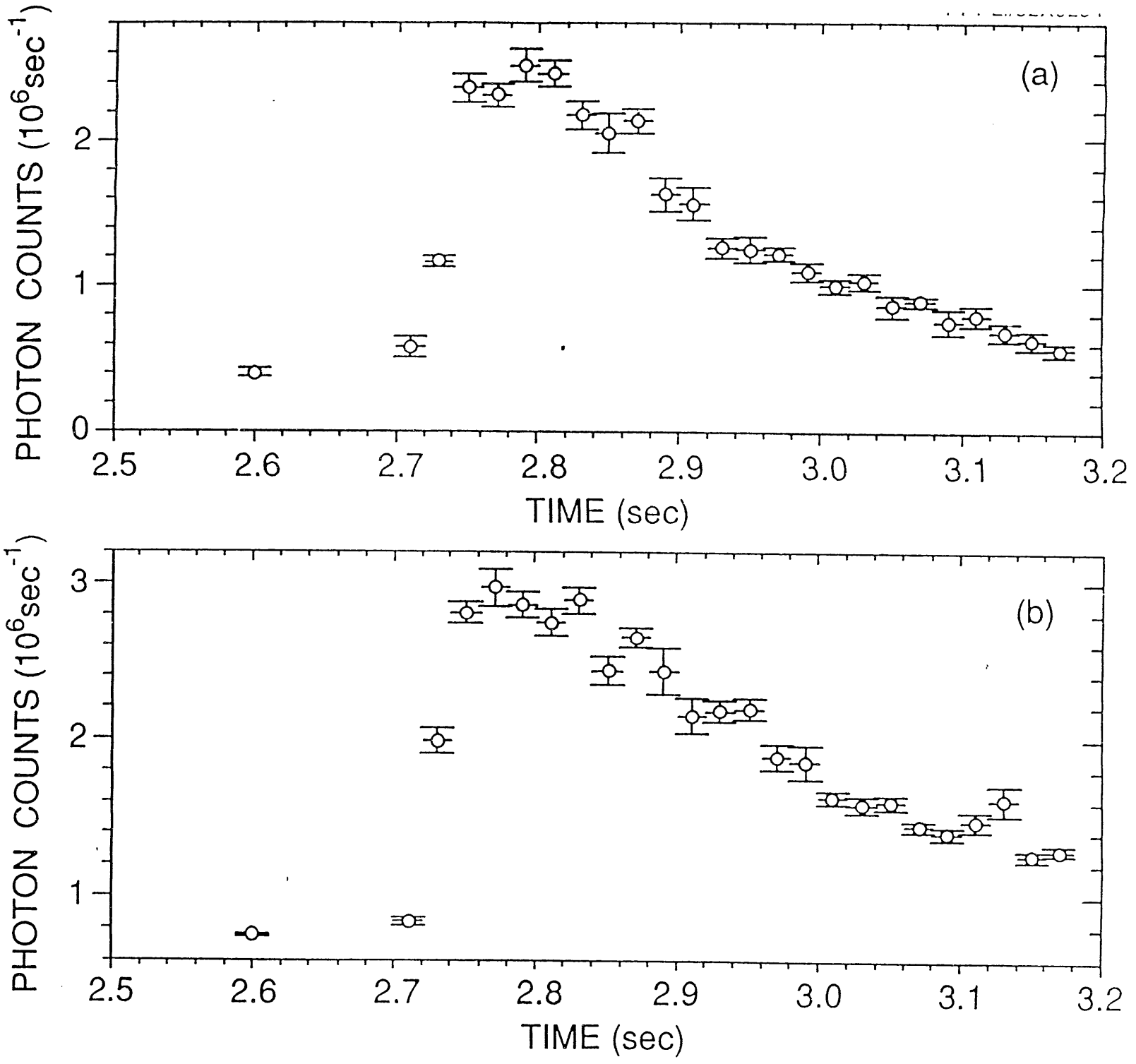
PHOTON COUNTS (10^6sec^{-1})
(a)
0
1
2
2.5
2.6
2.7
2.8
2.9
3.0
3.1
3.2
TIME (sec)
PHOTON COUNTS (10^6sec^{-1})
(b)
1
2
3
2.5
2.6
2.7
2.8
2.9
3.0
3.1
3.2
TIME (sec)

Figure 2

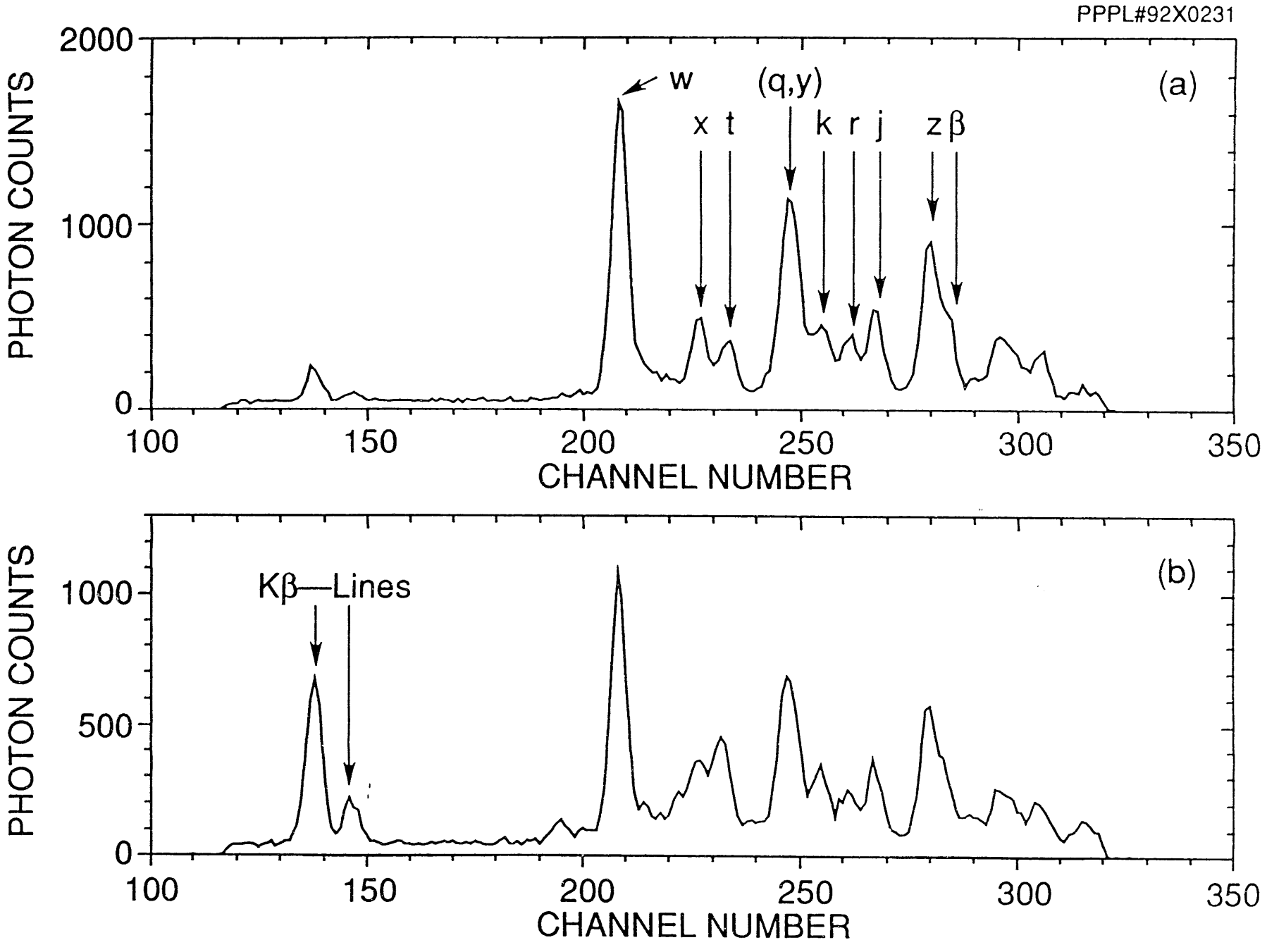
PPPL#92X0231
(a)
w
(q,y)
x t
k r j
z β
PHOTON COUNTS
2000
1000
0
100
150
200
250
300
350
CHANNEL NUMBER
(b)
Kβ—Lines
PHOTON COUNTS
1000
500
0
100
150
200
250
300
350
CHANNEL NUMBER

Figure 3

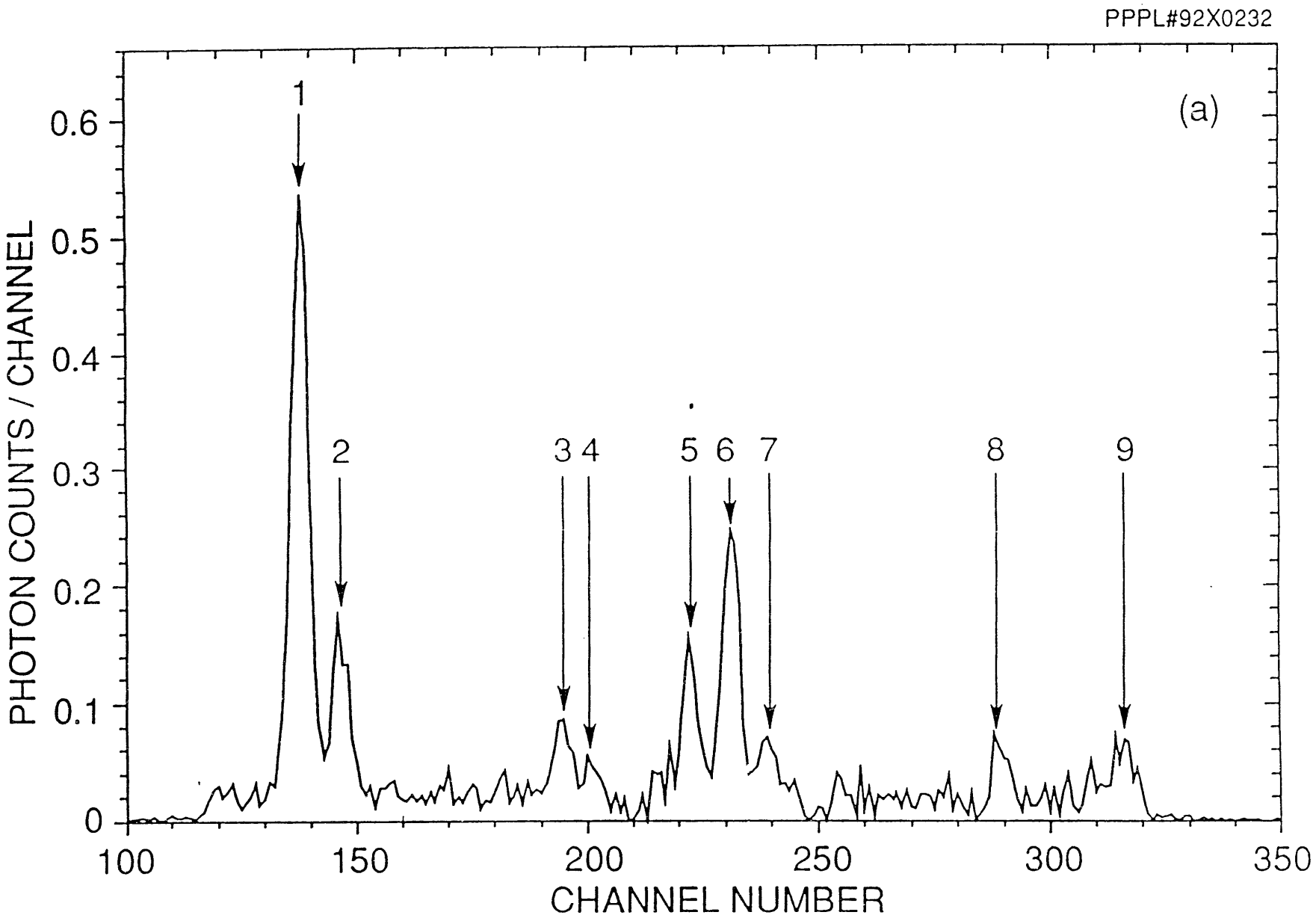
PPPL#92X0232
(a)
1
2
3 4
5 6 7
8
9
PHOTON COUNTS / CHANNEL
0
0.1
0.2
0.3
0.4
0.5
0.6
100
150
200
250
300
350
CHANNEL NUMBER

Figure 4

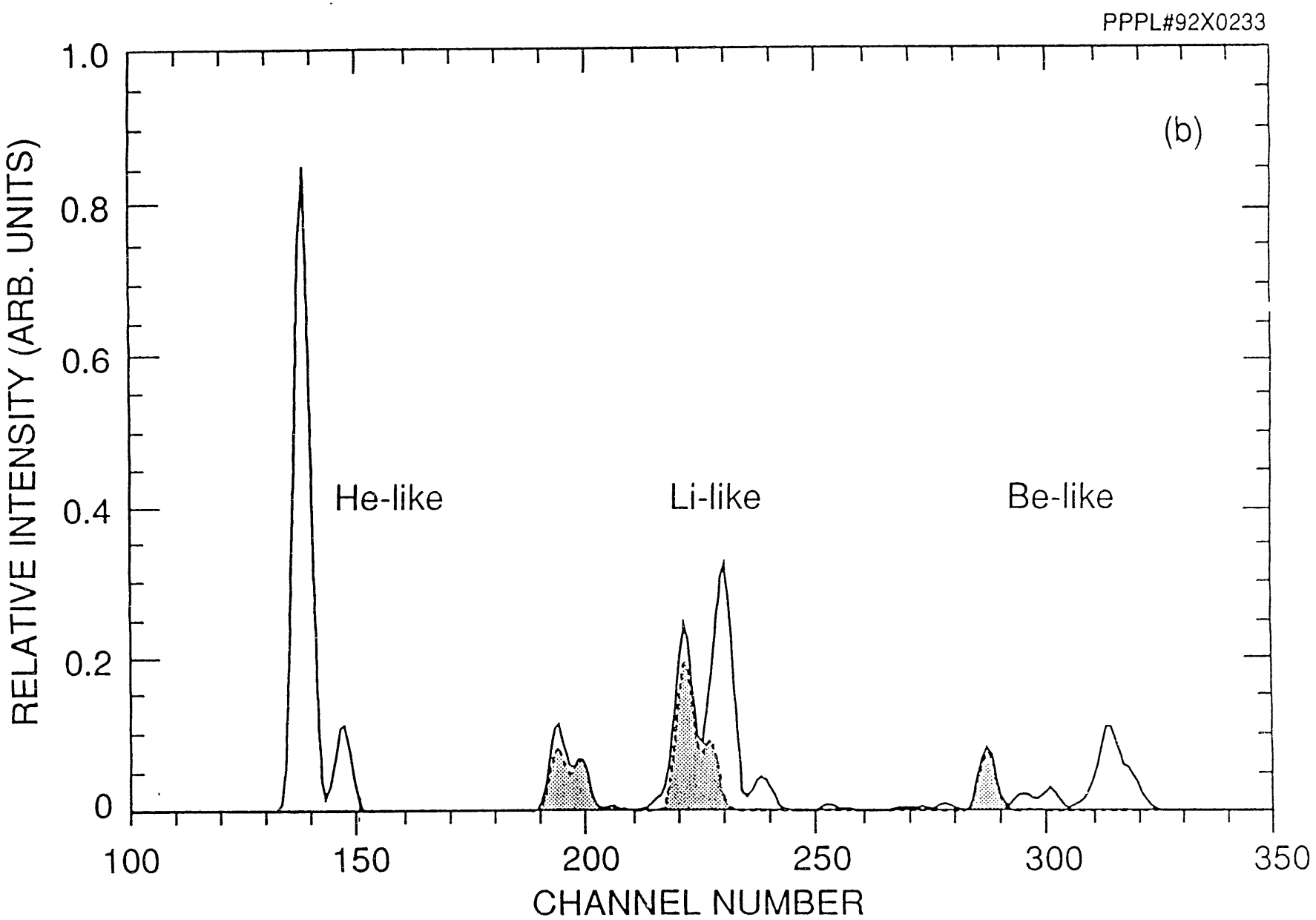
PPPL#92X0233
(b)
He-like
Li-like
Be-like
RELATIVE INTENSITY (ARB. UNITS)
1.0
0.8
0.6
0.4
0.2
0
100
150
200
250
300
350
CHANNEL NUMBER

Figure 4

EXTERNAL DISTRIBUTION IN ADDITION TO UC-420

Dr. F. Paoloni, Univ. of Wollongong, AUSTRALIA
Prof. M.H. Brennan, Univ. of Sydney, AUSTRALIA
Plasma Research Lab., Australian Nat. Univ., AUSTRALIA
Prof. I.R. Jones, Flinders Univ, AUSTRALIA
Prof. F. Cap, Inst. for Theoretical Physics, AUSTRIA
Prof. M. Heindler, Institut für Theoretische Physik, AUSTRIA
Prof. M. Goossens, Astronomisch Instituut, BELGIUM
Ecole Royale Militaire, Lab. de Phy. Plasmas, BELGIUM
Commission-European, DG. XII-Fusion Prog., BELGIUM
Prof. R. Boucique, Rijksuniversiteit Gent, BELGIUM
Dr. P.H. Sakanaka, Instituto Fisica, BRAZIL
Instituto Nacional De Pesquisas Espaciais-INPE, BRAZIL
Documents Office, Atomic Energy of Canada Ltd., CANADA
Dr. M.P. Bachynski, MPB Technologies, Inc., CANADA
Dr. H.M. Skarsgard, Univ. of Saskatchewan, CANADA
Prof. J. Teichmann, Univ. of Montreal, CANADA
Prof. S.R. Sreenivasan, Univ. of Calgary, CANADA
Prof. T.W. Johnston, INRS-Energie, CANADA
Dr. R. Bolton, Centre canadien de fusion magnétique, CANADA
Dr. C.R. James,, Univ. of Alberta, CANADA
Dr. P. Lukác, Komenského Universzita, CZECHO-SLOVAKIA
The Librarian, Culham Laboratory, ENGLAND
Library, R61, Rutherford Appleton Laboratory, ENGLAND
Mrs. S.A. Hutchinson, JET Library, ENGLAND
Dr. S.C. Sharma, Univ. of South Pacific, FIJI ISLANDS
P. Mähönen, Univ. of Helsinki, FINLAND
Prof. M.N. Bussac, Ecole Polytechnique,, FRANCE
C. Mouttet, Lab. de Physique des Milieux Ionisés, FRANCE
J. Radet, CEN/CADARACHE - Bat 506, FRANCE
Prof. E. Economou, Univ. of Crete, GREECE
Ms. C. Rinni, Univ. of Ioannina, GREECE
Dr. T. Mual, Academy Bibliographic Ser., HONG KONG
Preprint Library, Hungarian Academy of Sci., HUNGARY
Dr. B. DasGupta, Saha Inst. of Nuclear Physics, INDIA
Dr. P. Kaw, Inst. for Plasma Research, INDIA
Dr. P. Rosenau, Israel Inst. of Technology, ISRAEL
Librarian, International Center for Theo Physics, ITALY
Miss C. De Palo, Associazione EURATOM-ENEA , ITALY
Dr. G. Grosso, Istituto di Fisica del Plasma, ITALY
Prof. G. Rostangni, Istituto Gas Ionizzati Del Cnr, ITALY
Dr. H. Yamato, Toshiba Res & Devel Center, JAPAN
Prof. I. Kawakami, Hiroshima Univ., JAPAN
Prof. K. Nishikawa, Hiroshima Univ., JAPAN
Director, Japan Atomic Energy Research Inst., JAPAN
Prof. S. Itoh, Kyushu Univ., JAPAN
Research Info. Ctr., National Instit. for Fusion Science, JAPAN
Prof. S. Tanaka, Kyoto Univ., JAPAN
Library, Kyoto Univ., JAPAN
Prof. N. Inoue, Univ. of Tokyo, JAPAN
Secretary, Plasma Section, Electrotechnical Lab., JAPAN
S. Mori, Technical Advisor, JAERI, JAPAN
Dr. O. Mitarai, Kumamoto Inst. of Technology, JAPAN
J. Hyeon-Sook, Korea Atomic Energy Research Inst., KOREA
D.I. Choi, The Korea Adv. Inst. of Sci. & Tech., KOREA
Prof. B.S. Liley, Univ. of Waikato, NEW ZEALAND
Inst of Physics, Chinese Acad Sci PEOPLE'S REP. OF CHINA
Library, Inst. of Plasma Physics, PEOPLE'S REP. OF CHINA
Tsinghua Univ. Library, PEOPLE'S REPUBLIC OF CHINA
Z. Li, S.W. Inst Physics, PEOPLE'S REPUBLIC OF CHINA
Prof. J.A.C. Cabral, Instituto Superior Tecnico, PORTUGAL
Dr. O. Petrus, AL I CUZA Univ., ROMANIA
Dr. J. de Villiers, Fusion Studies, AEC, S. AFRICA
Prof. M.A. Hellberg, Univ. of Natal, S. AFRICA
Prof. D.E. Kim, Pohang Inst. of Sci. & Tech., SO. KOREA
Prof. C.I.E.M.A.T, Fusion Division Library, SPAIN
Dr. L. Stenflo, Univ. of UMEA, SWEDEN
Library, Royal Inst. of Technology, SWEDEN
Prof. H. Wilhelmson, Chalmers Univ. of Tech., SWEDEN
Centre Phys. Des Plasmas, Ecole Polytech, SWITZERLAND
Bibliotheek, Inst. Voor Plasma-Fysica, THE NETHERLANDS
Asst. Prof. Dr. S. Cakir, Middle East Tech. Univ., TURKEY
Dr. V.A. Glukhikh,Sci. Res. Inst. Electrophys.I Apparatus, USSR
Dr. D.D. Ryutov, Siberian Branch of Academy of Sci., USSR
Dr. G.A. Eliseev, I.V. Kurchatov Inst., USSR
Librarian, The Ukr.SSR Academy of Sciences, USSR
Dr. L.M. Kovrizhnykh, Inst. of General Physics, USSR
Kernforschungsanlage GmbH, Zentralbibliothek, W. GERMANY
Bibliothek, Inst. Für Plasmaforschung, W. GERMANY
Prof. K. Schindler, Ruhr-Universität Bochum, W. GERMANY
Dr. F. Wagner, (ASDEX), Max-Planck-Institut, W. GERMANY
Librarian, Max-Planck-Institut, W. GERMANY
Prof. R.K. Janev, Inst. of Physics, YUGOSLAVIA